

Article

Improved Heat Dissipation of Dip-Coated Single-Walled Carbon Nanotube/Mesh Sheets with High Flexibility and Free-Standing Strength for Thermoelectric Generators

Katsuma Miura ¹, Takuya Amezawa ¹, Saburo Tanaka ² and Masayuki Takashiri ^{1,*} ¹ Department of Materials Science, Tokai University, Hiratsuka 259-1292, Japan² Department of Mechanical Engineering, College of Engineering, Nihon University, Koriyama 963-8642, Japan; tanaka.saburo@nihon-u.ac.jp

* Correspondence: takashiri@tokai-u.jp

Abstract: Single-walled carbon nanotubes (SWCNTs) are promising thermoelectric materials used in thermoelectric generators (TEGs) to power sensors. However, the limitation of SWCNTs is their high thermal conductivity, which makes it difficult to create a sufficient temperature difference. In this study, we fabricated dip-coated SWCNT/mesh sheets using an SWCNT dispersion. Several types of mesh materials were tested, and the most suitable material was polyphenylene sulfide (PPS). SWCNTs were uniformly deposited on the PPS mesh surface without filling the mesh openings. The SWCNT/PPS mesh sheets exhibited flexibility and free-standing strength. When the edge of the SWCNT/PPS mesh sheets were heated, a higher temperature gradient was produced compared with that of the conventional SWCNT film owing to the increase in heat dissipation. A flexible and free-standing TEG with an area of 1200 mm², fabricated using SWCNT/PPS mesh sheets, exhibited an output voltage of 31.5 mV and maximum power of 631 nW at a temperature difference of 60 K (T_{low} : 320 K). When the TEG was exposed to wind at 3 m/s, temperature difference further increased, and the performance of the TEG increased by a factor of 1.3 for output voltage and 1.6 for maximum power. Therefore, we demonstrated that the TEG's performance could be improved using SWCNT/PPS mesh sheets.

Keywords: thermoelectric; single-walled carbon nanotube; mesh; dip-coat; heat dissipation

Citation: Miura, K.; Amezawa, T.; Tanaka, S.; Takashiri, M. Improved Heat Dissipation of Dip-Coated Single-Walled Carbon Nanotube/Mesh Sheets with High Flexibility and Free-Standing Strength for Thermoelectric Generators. *Coatings* **2024**, *14*, 126. <https://doi.org/10.3390/coatings14010126>

Academic Editors: Norbert M. Nemes and Carlos Jose Macedo Tavares

Received: 20 December 2023

Revised: 13 January 2024

Accepted: 16 January 2024

Published: 18 January 2024



Copyright: © 2024 by the authors. Licensee MDPI, Basel, Switzerland. This article is an open access article distributed under the terms and conditions of the Creative Commons Attribution (CC BY) license (<https://creativecommons.org/licenses/by/4.0/>).

1. Introduction

Carbon nanotubes (CNTs) have attracted significant attention as lightweight materials with excellent electrical conductivity, mechanical properties, and flexibility [1–4]. CNTs attached to a fibrous substrate have been proposed and used in various applications to take advantage of their beneficial properties [5–8]. CNTs are monolayer or multilayer cylindrical structures of six-membered ring networks (graphene sheets) made of carbon [9,10]. The properties of CNTs depend greatly on whether the cylindrical structure is a single-wall or multi-wall. Multi-walled CNTs (MWCNTs) exhibit metallic properties, whereas single-walled CNTs (SWCNTs) exhibit either metallic or semiconducting properties depending on their wrapping geometry [11,12]. Recently, the semiconducting properties of SWCNTs have been exploited in thermoelectric materials and generators [13–20].

Thermoelectric materials in thermoelectric generators (TEGs) produce electrical power through the Seebeck coefficient by applying a temperature difference between thermoelectric materials [21–25]. In particular, thin-film flexible TEGs are expected to be used as power sensors in cyber-physical systems (CPSs) and Internet of Things (IoT) technology [26–30]. The materials that exhibit the best thermoelectric performance near 300 K are bismuth telluride-based alloys [31–33]. However, the SWCNT film is a promising thermoelectric material owing to the aforementioned properties of CNTs as well as its relatively high thermoelectric properties (near 300 K) [34–36]. In addition, n-type SWCNTs with excellent

air stabilities have been developed, paving the way for all-carbon TEGs [37–43]. However, with current SWCNT sheets, it is challenging to create sufficient temperature differences within the sheets because the thermal conductivity of the SWCNTs is extremely high [44]. In addition, it is difficult to achieve excellent free-standing strength in SWCNT sheets when the sheet is extremely thin [45]. Therefore, when these two limitations are addressed, TEGs with SWCNT sheets are expected to become widely used as power supplies in CPS and IoT sensors.

In this study, we propose composite sheets with large temperature differences and excellent structural strength obtained by dip-coating SWCNTs onto a synthetic resin with a mesh structure. Dip-coating is an ideal method for preparing thin films from chemical solutions because it is a low-cost and waste-free process that can be easily scaled up and provides good control over the thickness of the film [46]. The composite sheets were characterized by a large number of through-holes penetrating in the direction of thickness and being free-standing with flexibility. Owing to their structure, the composite sheets have excellent structural strength and good heat dissipation properties because of the large surface area. The considerable temperature difference in the sheet was analyzed using computational fluid dynamics (CFD) and measured experimentally. Finally, flexible and free-standing TEGs were fabricated using the composite sheets, and their performances were measured by changing the temperature difference within the generators.

2. Materials and Methods

Materials: Single-walled carbon nanotubes (SWCNTs), also called super-growth carbon nanotubes (Zeon Co., Tokyo, Japan), were supplied by Zeon Corporation. An anionic surfactant of sodium dodecylbenzene sulfonate (SDBS) (Tokyo Chemical Industry, Tokyo, Japan) was used as received without further purification. Three types of mesh were used as follows: polyphenylene sulfide (PPS) with a sieve with 100 μm aperture and 34 μm wire diameter (Clever Co., Tokyo, Japan), polyvinyl chloride (PVC)-coated fiberglass with 1000 μm openings and 250 μm wire diameter (Clever Co.), and polypropylene (PP) of non-woven fabric mesh (C's One Co., Tokyo, Japan).

Preparation of dispersion: The dispersions were prepared by mixing the SWCNT and SDBS powders in deionized water using an ultrasonic homogenizer (SFX 250, Emerson Electric Co., St. Louis, MI, USA) operated at a maximum power of 200 W and amplitude of 30% for 30 min. The concentrations of SWCNT and sodium dodecyl benzene sulfonate (SDBS) in the dispersions were 0.2 and 1.0 wt%, respectively. To further increase the concentration, the dispersion was slowly heated to 358 K with stirring using a hot stirrer (NU32110, Kenis Co., Osaka, Japan) and kept at this temperature until the concentration of SWCNT and surfactant in the dispersion reached 0.5 and 2.5 wt%, respectively, by evaporating the water in the dispersion. The dispersion was then allowed to cool naturally in the air until it reached room temperature.

Analysis of SWCNT/mesh sheets: The surface morphologies of the SWCNT/mesh sheets were investigated using scanning electron microscopy (SEM) (S-4800, Hitachi, Tokyo, Japan) performed at an electron accelerating voltage of 3 kV. The in-plane Seebeck coefficient S of the SWCNT/mesh sheets was measured at approximately 300 K using a homemade device with an accuracy of $\pm 5\%$ [30]. One end of the thin film was connected to a heat sink and the other to a heater. The Seebeck coefficient was determined as the ratio of the potential difference across the membrane to the temperature difference measured with two 0.1 mm diameter K-type thermocouples pressed against the SWCNT/mesh sheet. The temperature difference between the thermocouples varied from 1 to 4 K, while the thermoelectric voltage was recorded at 1 K intervals using a temperature reader (GR-3500, KEYENCE, Osaka, Japan) and digital multimeter (R6561, ADVANTEST, Tokyo, Japan). The Seebeck coefficient was estimated from the V-K slope using a linear approximation. The in-plane electrical conductivity σ of the films was measured at approximately 300 K using a four-point probe method (RT-70V, Napson, Tokyo, Japan) with an accuracy of $\pm 5\%$ [47]. The in-plane power factor σS^2 was calculated from the experimentally measured Seebeck

coefficient and electrical conductivity. The temperature distribution of the SWCNT/mesh sheet was measured using a thermography camera (E5-XT, FLIR, Wilsonville, OR, USA).

Performance measurements of TEGs: The performance of the TEG was measured experimentally while the hotplate temperature was varied. The TEG was placed perpendicular to the hotplate (DP-1L, As One, Osaka, Japan) and fixed by securing its bottom edge between two glass substrates. The temperatures at the top and bottom of the TEG were measured using two K-type thermocouples. Two Cu-wire electrodes were connected to the outermost SWCNT films to measure the output voltage with an accuracy of $\pm 5\%$. The two thermocouples and two Cu wires were connected to a data logger (GL240-SD midi LOGGER, GRAPHTEC, Yokohama, Japan). The temperatures and output voltages at the top and bottom of the TEG were measured. The maximum power, P_{max} , was calculated from the output voltage V and the measured total electrical resistance of the TEG, R_{total} , as follows: $P_{max} = V^2 / 4R_{total}$.

3. Results and Discussion

3.1. Dip-Coated SWCNT/Mesh Sheets with Different Meshes

Figure 1 shows a schematic of the fabrication of the dip-coated SWCNT/mesh sheet and photographs of the different types of meshes before and after SWCNT dip-coating. We prepared three types of meshes: polyphenylene sulfide (PPS) mesh with a 100- μm aperture sieve, polyvinyl chloride (PVC)-coated glass-fiber mesh with a 1000- μm aperture sieve, and polypropylene (PP) of non-woven fabric mesh. Detailed specifications of the meshes are described in the Experimental Section. The meshes were slowly immersed in a dispersion containing 0.5 wt% SWCNTs and 2.5 wt% anionic surfactant of sodium dodecylbenzene sulfonate (SDBS). After removing the dip-coated SWCNT/mesh sheets from the dispersion, they were dried in a natural convection oven (DY400, Tokyo, Japan) at 333 K for 24 h. When the PPS mesh was used, the SWCNTs appeared to coat the mesh surface, and the mesh did not wrinkle. However, in the PVC-coated glass-fiber mesh, the SWCNTs were unable to coat the mesh surface owing to the high hydrophobicity of PVC. In the PP of the nonwoven fabric mesh, the SWCNTs could coat the mesh surface, but the SWCNTs/PP shrank and wrinkled.

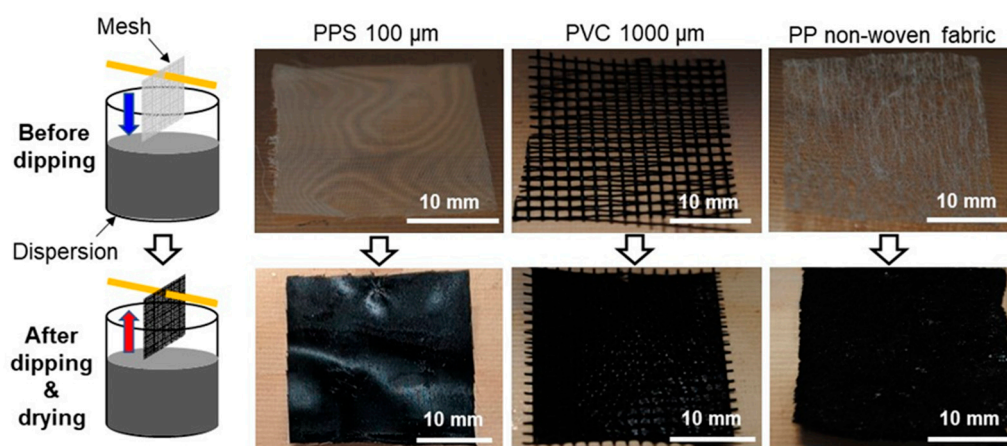


Figure 1. Schematic of the fabrication of dip-coated SWCNT/mesh sheets and photographs of different types of meshes before and after SWCNT dip-coating.

The thermoelectric and structural properties of the SWCNT/mesh sheets with different mesh types are listed in Table 1. The SWCNT/PPS mesh exhibited an electrical conductivity σ of 7.2 S/cm, a Seebeck coefficient S of 61.9 $\mu\text{V}/\text{K}$, and a power factor σS^2 of 2.8 $\mu\text{W}/(\text{m}\cdot\text{K}^2)$. In addition, the SWCNT/PPS mesh exhibits sufficient flexibility and free-standing strength. Compared with the thermoelectric properties of the SWCNT buckypaper prepared by vacuum filtering with a similar dispersion containing SWCNTs and SDBS [17], the electrical conductivity of the SWCNT/PPS mesh was lower than that of the

buckypaper because the SWCNT/PPS mesh sheet was expected to have a porous structure, and the electric current flowed through the SWCNTs but not through the PPS mesh. For the SWCNT/PVC mesh sheet, the thermoelectric and structural properties were not measured owing to no SWCNT coating on the PVC surface. For the SWCNT/PP mesh sheet, the Seebeck coefficient was lower than that of the SWCNT/PPS mesh sheet. The SWCNT/PP mesh sheet exhibited flexibility, but its free-standing strength was poor compared with that of the SWCNT/PPS mesh sheet. Therefore, we conclude that the PPS mesh is most suitable for fabricating SWCNT/mesh TEGs.

Table 1. Thermoelectric and structural properties of SWCNT/mesh sheets with different mesh types. For comparison, properties of SWCNT buckypaper are added as a reference.

Mesh Type	σ [S/cm]	S [$\mu\text{V/K}$]	σS^2 [$\mu\text{W}/(\text{m}\cdot\text{K}^2)$]	Flexibility	Free-Standing Strength	Ref.
SWCNT/PPS-mesh	7.2	61.9	2.8	Excellent	Excellent	This work
SWCNT/PVC-mesh		No evaluation due to incomplete coating				This work
SWCNT/PP-mesh	7.4	48.1	1.7	Excellent	Poor	This work
SWCNT buckypaper	41	53	12	Excellent	Average	[17]

3.2. SWCNT/Mesh Sheets with Various Dip-Coatings

Based on the results in Section 3.1, we focused on the PPS mesh to fabricate SWCNT/mesh sheets to increase the amount of SWCNTs. For this purpose, the dip-coating and drying processes were repeated up to three times. The scanning electron micrography (SEM) images of the SWCNT/PPS mesh sheets are shown in Figure 2. The PPS wire before SWCNT dip-coating is shown in Figure 2a; the SWCNT/PPS mesh sheet exhibited free-standing strength. In Figure 2b, in one dip-coating, corresponding to the description in Section 3.1, SWCNTs were deposited on the PPS mesh surface. A high-magnification SEM image is provided in the Supplementary Information (Figure S1). The SWCNTs uniformly covered the PPS wires without cracks. As the number of dip-coatings increased, the wire diameters also increased (Figure 2c–d). Although the amount of SWCNTs deposited on the mesh increased with the number of dip-coatings, the openings in the mesh were not filled with SWCNTs. Therefore, we demonstrated the fabrication of SWCNT/PPS mesh sheets with desired shapes.

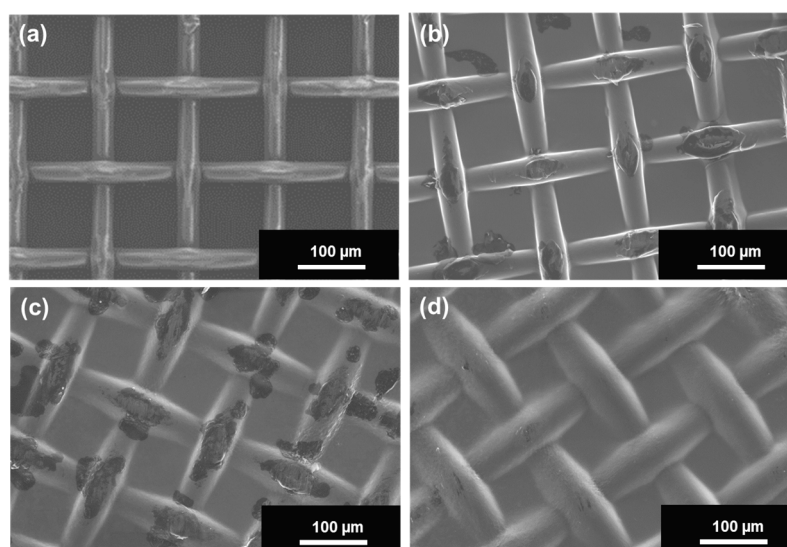


Figure 2. Surface morphologies of SWCNT/PPS mesh sheets with different numbers of dip-coatings: (a) PPS mesh sheet, SWCNT/PPS mesh sheets with (b) one dip-coating, (c) two dip-coatings, and (d) three dip-coatings.

Table 2 lists the structural and thermoelectric properties of the SWCNT/PPS mesh sheets with different numbers of dip-coatings. Based on the SEM images in Figure 2a–d, the diameter of the PPS wire before SWCNT dip-coating was determined to be 34 μm . The approximate wire diameters of the one, two, and three dip-coatings were 40, 52, and 60 μm , respectively. The thickness of the SWCNTs on the PPS mesh was calculated by assuming that the SWCNTs were uniformly deposited on the mesh surface. The thickness of the SWCNTs was approximately 3 μm with one dip-coating, which increased to 13 μm with three dip-coatings. The flexibility of the SWCNT/PPS mesh sheets was investigated by bending tests; the results showed that the sheet with one dip-coating had excellent flexibility, which deteriorated as the number of dip-coatings increased. When the coating was performed thrice, the cracks were formed in the SWCNTs by bending. The SWCNT/PPS mesh sheets with one and two dip-coatings exhibited similar values, which were 7 S/cm for electrical conductivity, 60 $\mu\text{V}/\text{K}$ for p-type Seebeck coefficient, and 3 $\mu\text{W}/(\text{m}\cdot\text{K}^2)$ for power factor. However, the thermoelectric properties of the SWCNT/PPS mesh sheet with three dip-coatings were not measured because of the cracks in the SWCNTs. Therefore, we conclude that the SWCNT/PPS mesh sheet with one dip-coating is the most suitable for fabricating flexible and free-standing SWCNT/mesh TEGs.

Table 2. Structural and thermoelectric properties of SWCNT/PPS mesh sheets with different numbers of dip-coatings.

Numbers of Dip-Coating at SWCNT/PPS	Wire Diameter [μm]	SWCNT Thickness [μm]	* Flexibility	σ [S/cm]	S [$\mu\text{V}/\text{K}$]	σS^2 [$\mu\text{W}/(\text{m}\cdot\text{K}^2)$]
One	40	3	Excellent	7.2	61.9	2.8
Two	52	9	Average	7.4	63.2	3.0
Three	60	13	Poor	Not measurable due to cracking		

* Flexibility: Excellent = Equivalent to PPS sheet; Average = Not equal to PPS sheet, but flexible; Poor = Inflexible, cracks by bending.

To investigate the durability of the SWCNT/PPS mesh sheet with the one dip-coating, repeated bending and adhesion tests were performed [48–50]. For the bending test, the process of bending and unbending the sheet along a 10-mm radius tube was repeated for 600 cycles, and the thermoelectric properties were measured every 100 cycles. Figure 3a shows that the Seebeck coefficient was nearly constant over the range of 0–600 cycles. However, the electrical conductivity decreased by approximately 20% compared with the initial value. For the adhesion test, standardized tape was attached to the sheet and pulled off with a constant force, as shown in Figure 3b. When the adhesion test was repeated five times, no delamination of SWCNTs was observed until the fourth test; however, delamination is observed in the fifth test. Therefore, their durability should be improved by modifying the PPS mesh surface [51–55].

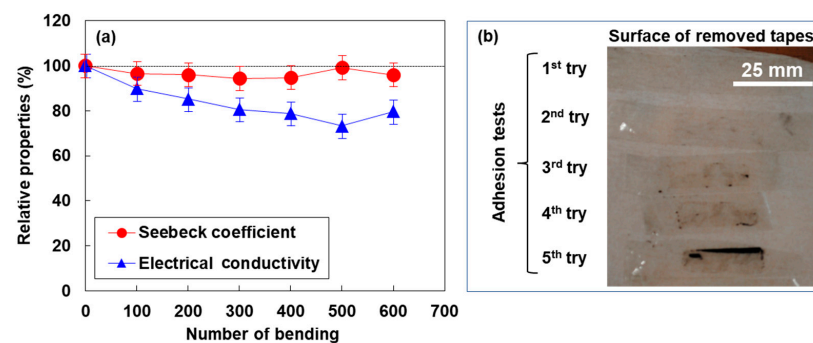


Figure 3. (a) Relative Seebeck coefficient and electrical conductivity of SWCNT/PPS mesh sheets with one dip-coating as a function of the number of bends. (b) Photographs of SWCNT/PPS mesh sheets in adhesion tests repeated five times.

To investigate the heat dissipation in the SWCNT/PPS mesh sheets, we measured the temperature distribution via local heating of the sheets. A schematic of the temperature distribution measurement of the SWCNT/PPS mesh sheets is shown in Figure 4a. The bottom of the SWCNT/PPS mesh sheet was fixed to a hotplate, and the temperature was maintained at 333 K; moreover, the temperature distribution of the sheets under steady-state conditions was measured using a thermography camera. In Figure 4b, the temperature distribution of the SWCNT/PPS mesh sheet with one dip-coating is compared with that of the SWCNT buckypaper with a similar thickness (40 μm); the results showed that the SWCNT/PPS mesh sheet was more prone to temperature gradients than SWCNT buckypaper. This difference occurred because the SWCNT/PPS mesh sheets had lower thermal conductivity and larger surface area than the SWCNT buckypaper. Notably, we confirmed the stability of the temperature distributions in both the samples by continuous measurement for 1 h. As a result, the SWCNT/PPS mesh sheets facilitated heat dissipation. To investigate the effect of the presence or absence of sieve openings in the SWCNT/PPS mesh sheets, we prepared the PPS film without sieve openings and fabricated an SWCNT/PPS film using the same process with a similar film thickness. The measured temperature distributions of the SWCNT/PPS mesh sheet and SWCNT/PPS film are shown in Figure 4c. The results indicate that the SWCNT/PPS mesh sheet produced a higher temperature gradient than the SWCNT/PPS film. Consequently, the sieve openings in the PPS mesh contributed to an increase in heat dissipation, and this event was confirmed by a CFD study, as provided in the Supplementary Information (Figures S2 and S3). The temperature distributions of the SWCNT/PPS mesh sheets with different numbers of dip-coatings are shown in Figure 4d. As the number of dip-coatings increased, temperature gradients in the SWCNT/PPS mesh sheets were less likely to occur because multiple dip-coatings increased the thermal conductivity of the SWCNT/PPS mesh sheet by increasing the proportion of SWCNTs with high thermal conductivity; the heat dissipation was limited by reducing the sieve opening area of the mesh. Therefore, based on the temperature distribution measurements, we conclude that the SWCNT/PPS mesh sheet with one dip-coating is highly suitable for use in TEGs.

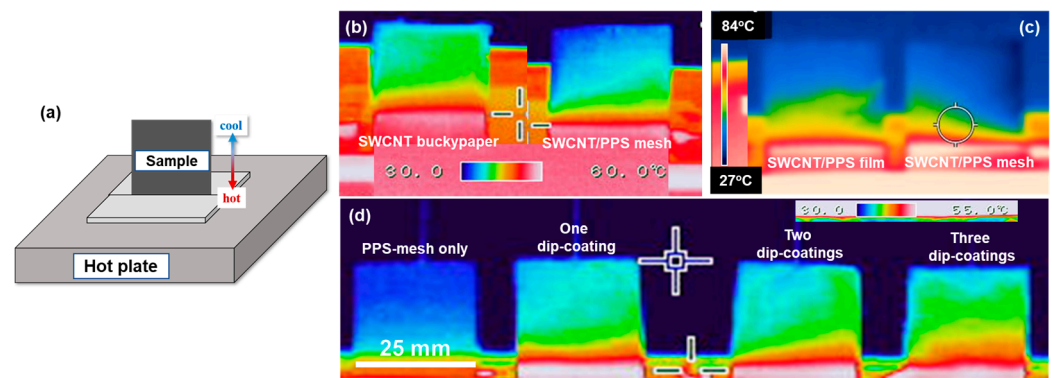


Figure 4. Temperature distributions of SWCNT/PPS mesh sheet with one dip-coating and reference samples. (a) Schematic of measuring the temperature distribution using a thermography camera, (b) SWCNT/PPS mesh sheet and SWCNT buckypaper, (c) SWCNT/PPS mesh sheet and SWCNT/PPS film, and (d) SWCNT/PPS mesh sheets with different numbers of dip-coatings. Note that all images of the samples in (b–d) are the same size.

3.3. TEGs Using Dip-Coated SWCNT/Mesh Sheets

Based on the results in Section 3.2, we fabricated TEGs using SWCNT/PPS mesh sheets with one dip-coating and measured their performance. A schematic of the fabrication of TEGs is shown in Figure 5. First, a piece of masking tape was applied to a PPS mesh sheet to ensure that the SWCNTs were coated only on the desired areas, allowing the creation of eight independent SWCNT-coated areas. Subsequently, the PPS mesh sheet was slowly dipped into the SWCNT dispersion solution. After the dipping, the SWCNT/PPS

mesh sheets were dried in a natural convection oven at 333 K for 24 h. When the masking tape was removed from the sheet, striped SWCNT patterns were formed. The SWCNT-coated areas were arranged in four horizontal and two vertical rows. Because the SWCNTs used in this study exhibited p-type properties, the lower and upper edges of the adjacent SWCNT-coated areas were connected via thin copper wires to ensure that the areas were connected in series. The connection method used for the TEG was a long and thin copper wire sewn into a mesh sheet. In addition, silver paste was applied to the junctions to reduce the contact resistance between the SWCNTs and thin copper wires. Finally, the TEG was completed by mountain-folding the central part of the SWCNT/PPS mesh sheet, and a polyimide sheet was inserted between the bent SWCNT/PPS mesh sheets to prevent them from touching each other. A photograph of the completed TEG is shown in Figure 5. The overall dimensions of the TEG are 30 mm wide and 20 mm long with the bend, and the dimensions of the SWCNT-coated area were 6 mm wide and 20 mm long.

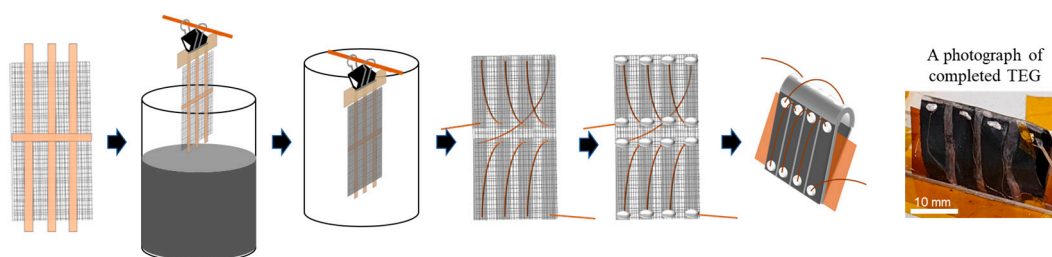


Figure 5. Schematic of the fabrication of a TEG with dip-coated SWCNT/mesh sheet and photograph of a completed TEG.

Figure 6 shows the performance of the TEG with SWCNT/PPS mesh sheets. The bottom end of the TEG was fixed on a hotplate; the output voltage and temperatures of the top and bottom ends of the TEG were measured, while the temperature at the bottom end of the sheet was varied from 303 to 373 K. The total resistance of the TEG was almost constant at 441 Ω at the temperature range in this measurement condition, as provided in Supplementary Information (Figure S4). As shown in Figure 6a, the output voltage and maximum power increased with the temperature difference between the top and bottom ends of the TEG. When the temperature difference was 60 K and the temperature at the bottom end of the sheet was 373 K, the output voltage and maximum power were 31.5 mV and 631 nW, respectively. Based on the value of the Seebeck coefficient ($S = -61.9 \mu\text{V}/\text{K}$) of SWCNT/PPS mesh films (one dip-coating), the output voltage was calculated under the same conditions as the TEG. When the temperature difference was applied to 60 K, the calculated output voltage was 29.7 mV while the measured output voltage of the TEG was 31.5 mV. Therefore, the properties (Seebeck coefficient) of the SWCNT/PPS mesh films are directly reflected in the performance (output voltage) of the TEG. Generally, the lowest voltage at which booster circuits can be used is 20 mV [56]; this can be achieved by the TEG at a temperature difference of 35 K. In this study, we compared the temperature difference of the TEG with SWCNT/PPS mesh sheets with that of the TEG with SWCNT buckypaper on polyimide film at the same temperature as the bottom ends of the TEGs with the same SWCNT length of 20 mm [17]. When the bottom ends of the TEGs were at 343 K, the temperature difference of 27 K was exhibited in the TEG with SWCNT/PPS mesh sheets, whereas that of 21 K was exhibited in the TEG with SWCNT buckypaper on polyimide film. Under these conditions, the output voltage and maximum power of the TEG with SWCNT/PPS mesh sheets were 15.6 mV and 148 nW, respectively. Meanwhile, the output voltage and maximum power of the TEG with SWCNT buckypaper on polyimide film were 8.3 mV and 164 nW, respectively. Notably, the TEG of the SWCNT buckypaper on the polyimide film consisted of two p-n pairs (four SWCNTs in total); therefore, the performance was doubled in comparison with the TEG of the SWCNT/PPS mesh sheet, which consisted of eight p-type SWCNTs. As a result, the TEG with the SWCNT/PPS mesh sheet exhibited 1.9 times higher output voltage, but the maximum power was slightly

lower than that of the TEG with the SWCNT buckypaper on the polyimide film. This is attributed to the fact that the TEG with the SWCNT/PPS mesh sheet had a relatively high electrical resistance of 441Ω , whereas that of the SWCNT buckypaper on the polyimide film was estimated to be 92Ω . In future studies, the electrical resistance should be reduced without compromising the flexibility, and the thermoelectric performance should be further increased to optimize the TEG structures [17,30]. As shown in Figure 6b, we measured the performance of the TEG in wind at 3 m/s using a circulator. This measurement was performed under the assumption that the TEG would be used outdoors by exposing it to a wind speed of 3 m/s. Heat dissipation was further increased by blowing air, and the temperature difference in the TEG increased to 80 K when the temperature at the bottom end of the sheet was 373 K. Under these conditions, the output voltage and maximum power were 41 mV and 1023 nW, respectively. Compared with the performance of a TEG without wind at the same temperature as the bottom end of the sheet, the performance of the TEG with wind increased by a factor of 1.3 for output voltage and 1.6 for maximum power.

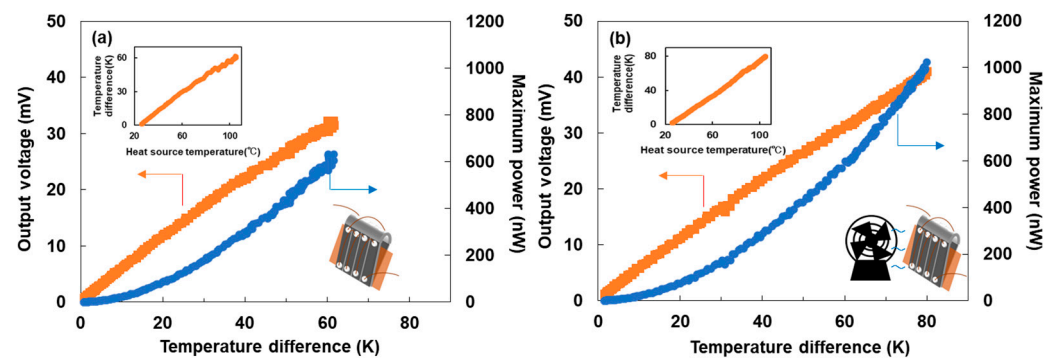


Figure 6. Output voltage and maximum power of a TEG with a dip-coated SWCNT/mesh sheet as a function of temperature difference: (a) Normal condition and (b) blowing wind at 3 m/s.

4. Conclusions

Dip-coated SWCNT/mesh sheets were prepared for high-performance TEGs. Among mesh materials such as PPS, PVC, and PP, the most suitable material was PPS. SWCNTs were uniformly deposited on the PPS mesh surface without filling the mesh openings. In particular, the SWCNT/PPS mesh sheet with an SWCNT thickness of approximately $3 \mu\text{m}$ exhibited flexibility and free-standing strength. To investigate the heat dissipation of the SWCNT/PPS mesh sheets, the temperature distribution was measured by heating the edge of the sheets. The SWCNT/PPS mesh sheet was more prone to temperature gradients than the conventional SWCNT buckypaper owing to the increase in heat dissipation. When the TEG was fabricated with SWCNT/PPS mesh sheets, it exhibited an output voltage of 31.5 mV and a maximum power of 631 nW at a temperature difference of 60 K. Furthermore, when the TEG was exposed to a 3 m/s wind, the temperature difference increased to 80 K and the performance of the TEG increased. Therefore, we concluded that the performance of the TEG could be improved using the SWCNT/PPS mesh. This achievement can potentially lead to the widespread use of TEGs as power sources for CPS and IoT sensors.

Supplementary Materials: The following supporting information can be downloaded at <https://www.mdpi.com/article/10.3390/coatings14010126/s1>, Figure S1: Higher magnification SEM image of SWCNT/PPS mesh sheet with one dip-coating. The SWCNTs uniformly covered the PPS wires without cracks.; Figure S2: Model for CFD.; Figure S3: Comparison of temperature distribution of PPS and CNT. (a) Mesh structure and (b) no mesh structure.; Figure S4: Total resistance of TEG using SWCNT/PPS mesh sheet as a function of average temperature of TEG. The total resistance of TEG was almost constant at 441Ω at the temperature range in this measurement condition.; Table S1: Properties of the gas and material.

Author Contributions: K.M. and M.T. conceived this study and designed the experiments. K.M. and M.T. wrote the main manuscript. The experiments and data analysis were performed by K.M. and T.A. with help from M.T. CFD analysis was performed by S.T. All authors have read and agreed to the published version of the manuscript.

Funding: This research was funded by Soken Project at Tokai University, grant number PJ2022-1, and Hiratsuka City Industry-Academia Joint Research Commercialization Support Grant.

Institutional Review Board Statement: Not applicable.

Informed Consent Statement: Not applicable.

Data Availability Statement: Research data can be shared by M.T., if requested.

Acknowledgments: All authors thank H. Uchida and K. Nishiura at Zeon Corporation for providing SG-CNT powders, as well as M. Morikawa, Y. Oda, K. Hoshino, and H. Yamamoto at Tokai University for experimental support.

Conflicts of Interest: The authors declare no conflict of interest.

References

1. Ma, Z.; Wei, A.; Ma, J.; Shao, L.; Jiang, H.; Dong, D.; Ji, Z.; Wang, Q.; Kang, S. Lightweight, compressible and electrically conductive polyurethane sponges coated with synergistic multiwalled carbon nanotubes and graphene for piezoresistive sensors. *Nanoscale* **2018**, *10*, 7116. [PubMed]
2. Hu, P.; Lyu, J.; Fu, C.; Gong, W.-B.; Liao, J.; Lu, W.; Chen, Y.; Zhang, X. Multifunctional aramid nanofiber/carbon nanotube hybrid aerogel films. *ACS Nano* **2022**, *14*, 688. [CrossRef]
3. Wang, C.; Xia, K.; Wang, H.; Liang, X.; Yin, Z.; Zhang, Y. Advanced carbon for flexible and wearable electronics. *Adv. Mater.* **2019**, *31*, 1801072. [CrossRef]
4. Nguyen, N.; Zhang, S.; Oluwalowa, A.; Park, J.G.; Yao, K.; Liang, R. High-performance and lightweight thermal management devices by 3D printing and assembly of continuous carbon nanotube sheets. *ACS Appl. Mater. Interfaces* **2018**, *10*, 27171.
5. Dai, H. Carbon nanotubes: Opportunities and challenges. *Surf. Sci.* **2002**, *500*, 218. [CrossRef]
6. Mamalis, A.G.; Vogtländer, G.O.L.; Markopoulos, A. Nanotechnology and nanostructured materials: Trends in carbon nanotubes. *Precis. Eng.* **2004**, *28*, 16.
7. Huang, X.; Yin, Z.; Wu, S.; Qi, X.; He, Q.; Zhang, Q.; Yan, Q.; Boey, F.; Zhang, H. Graphene-based materials: Synthesis, characterization, properties, and applications. *Small* **2011**, *7*, 1876.
8. Hossain, M.M.; Li, B.M.; Sennik, B.; Jur, J.S.; Bradford, P.D. Adhesive free, conformable and washable carbon nanotube fabric electrodes for biosensing. *npj Flexible Electron.* **2022**, *6*, 97.
9. Iijima, S. Helical microtubules of graphitic carbon. *Nature* **1991**, *354*, 56.
10. Jafari, Z.; Avargani, V.M.; Rahimi, M.R.; Mosleh, S. Magnetic nanoparticles-embedded nitrogen-doped carbon nanotube/porous carbon hybrid derived from a metal-organic framework as a highly efficient adsorbent for selective removal of Pb(II) ions from aqueous solution. *J. Mol. Liq.* **2020**, *318*, 113987. [CrossRef]
11. Tang, D.-M.; Erohin, S.V.; Kvashnin, D.G.; Demin, V.A.; Cretu, O.; Jiang, S.; Zhang, L.; Hou, P.X.; Chen, G.; Futaba, D.N.; et al. Semiconductor nanochannels in metallic carbon nanotubes by thermomechanical chirality alteration. *Science* **2021**, *374*, 1616. [CrossRef] [PubMed]
12. Tanaka, T.; Liu, H.; Fuji, S.; Kataura, H. From metal/semiconductor separation to single-chirality separation of single-wall carbon nanotubes using gel. *Phys. Status Solidi RRL* **2011**, *5*, 301. [CrossRef]
13. Choi, J.; Jung, Y.; Yang, S.J.; Oh, J.Y.; Oh, J.; Jo, K.; Son, J.G.; Moon, S.E.; Park, C.R.; Kim, H. Flexible and robust thermoelectric generators based on all-carbon nanotube yarn without metal electrodes. *ACS Nano* **2017**, *11*, 7608. [CrossRef]
14. Blackburn, J.L.; Ferguson, A.J.; Cho, C.; Grunlan, J.C. Carbon-nanotube-based thermoelectric materials and devices. *Adv. Mater.* **2018**, *30*, 1704386. [CrossRef] [PubMed]
15. Zhang, Y.; Zhang, Q.; Chen, G. Carbon and carbon composites for thermoelectric applications. *Carbon Energy* **2020**, *2*, 408. [CrossRef]
16. Chiba, T.; Amma, Y.; Takashiri, M. Heat source free water floating carbon nanotube thermoelectric generators. *Sci. Rep.* **2021**, *11*, 14707. [CrossRef] [PubMed]
17. Konagaya, R.; Takashiri, M. Dual-type flexible-film thermoelectric generators using all-carbon nanotube films. *Coatings* **2023**, *13*, 13209. [CrossRef]
18. Mytafides, C.K.; Tzounis, L.; Karalis, G.; Formanek, P.; Paipetis, A.S. High-power all-carbon fully printed and wearable SWCNT-based organic thermoelectric generator. *ACS Appl. Mater. Interfaces* **2021**, *13*, 11151–11165. [CrossRef]
19. Vareli, I.; Tzounis, L.; Tsirka, K.; Kavvadias, I.E.; Tsongas, K.; Liebscher, M.; Elenas, A.; Gergidis, L.N.; Barkoula, N.-M.; Paipetis, A.S. High-performance cement/SWCNT thermoelectric nanocomposites and a structural thermoelectric generator device towards large-scale thermal energy harvesting. *J. Mater. Chem. C* **2021**, *9*, 14421–14438. [CrossRef]

20. Macleod, B.A.; Stanton, N.J.; Gould, I.E.; Wesenberg, D.; Ihly, R.; Owczarczyk, Z.R.; Hurst, K.E.; Fewox, C.S.; Folmar, C.N.; Hughes, K.H.; et al. Large n- and p-type thermoelectric power factors from doped semiconducting single-walled carbon nanotube thin films. *Energy Environ. Sci.* **2017**, *10*, 2168–2179. [[CrossRef](#)]
21. Khongthong, J.; Raginov, J.N.; Khabushev, E.M.; Goldt, A.E.; Kondrashov, V.A.; Russakov, D.M.; Shandakov, S.D.; Krasnikov, D.V.; Nasibulin, A.G. Aerosol doping of SWCNT films with p- and n-type dopants for optimizing thermoelectric performance. *Carbon* **2024**, *218*, 118670. [[CrossRef](#)]
22. Wada, K.; Tomita, K.; Takashiri, M. Fabrication of bismuth telluride nanoplates via solvothermal synthesis using different alkalis and nanoplate thin films by printing method. *J. Cryst. Growth* **2017**, *468*, 194–198.
23. Liu, Y.; Du, Y.; Meng, Q.; Xu, J.; Shen, S.Z. Effects of preparation methods on the thermoelectric performance of SWCNT/Bi₂Te₃ bulk composites. *Materials* **2020**, *13*, 2636. [[PubMed](#)]
24. Zoui, M.A.; Bentouba, S.; Stocholm, J.G.; Bourouis, M. A review on thermoelectric generators: Progress and applications. *Energies* **2020**, *13*, 3606. [[CrossRef](#)]
25. Toan, N.V.; Truong, T.T.K.; Ono, T. Thermoelectric generators for heat harvesting: From material synthesis to device fabrication. *Energy Convers. Manage.* **2020**, *225*, 113442.
26. Lee, E.A. The past, present and future of cyber-physical systems: A focus on models. *Sensors* **2015**, *15*, 4837.
27. Du, Y.; Xua, J.; Paul, B.; Eklund, P. Flexible thermoelectric materials and devices. *App. Mater. Today* **2018**, *12*, 366. [[CrossRef](#)]
28. Karthikeyan, V.; Surjadi, J.U.; Wong, J.C.K.; Kannan, V.; Lam, K.-H.; Chen, X.; Lu, Y.; Roy, V.A.L. Wearable and flexible thin film thermoelectric module for multi-scale energy harvesting. *J. Power Sources* **2020**, *455*, 227983.
29. Wang, Y.; Zhu, W.; Deng, Y.; Fu, B.; Zhu, P.; Yu, Y.; Li, J.; Guo, J. Self-powered wearable pressure sensing system for continuous healthcare monitoring enabled by flexible thin-film thermoelectric generator. *Nano Energy* **2020**, *73*, 075216.
30. Kobayashi, A.; Konagaya, R.; Tanaka, S.; Takashiri, M. Optimized structure of tubular thermoelectric generators using n-type Bi₂Te₃ and p-type Sb₂Te₃ thin films on flexible substrate for energy harvesting. *Sens. Actuators A* **2020**, *313*, 112199. [[CrossRef](#)]
31. Liu, W.-D.; Yin, L.-C.; Li, L.; Yang, Q.; Wang, D.-Z.; Li, M.; Shi, X.-L.; Liu, Q.; Bai, Y.; Gentle, I.; et al. Grain boundary recrystallization and sub-nano regions leading to high plateau figure of merit for Bi₂Te₃ nanoflakes. *Energy Environ. Sci.* **2023**, *16*, 5123–5135. [[CrossRef](#)]
32. Kato, K.; Hatasako, Y.; Uchino, M.; Nakata, Y.; Suzuki, Y.; Hayakawa, T.; Adachi, C.; Miyazaki, K. Flexible porous bismuth telluride thin films with enhanced figure of merit using micro-phase separation of block copolymer. *Adv. Mater. Interfaces* **2014**, *1*, 1300015. [[CrossRef](#)]
33. Kashiwagi, M.; Hirata, S.; Harada, K.; Zheng, Y.; Miyazaki, K.; Yahiro, M.; Adachi, C. Enhanced figure of merit of a porous thin film of bismuth antimony telluride. *Appl. Phys. Lett.* **2011**, *98*, 023114. [[CrossRef](#)]
34. Avery, A.D.; Zhou, B.H.; Lee, J.; Lee, E.-S.; Miller, E.M.; Ihly, R.; Wesenberg, D.; Mistry, K.S.; Guillot, S.L.; Zink, B.L.; et al. Tailored semiconducting carbon nanotube networks with enhanced thermoelectric properties. *Nat. Energy* **2016**, *1*, 16033. [[CrossRef](#)]
35. Hasan, M.N.; Nafea, M.; Nayan, N.; Ali, M.S.M. Thermoelectric generator: Materials and applications in wearable health monitoring sensors and Internet of Things devices. *Adv. Mater. Technol.* **2021**, *7*, 2101203. [[CrossRef](#)]
36. Komatsu, N.; Ichinose, Y.; Dewey, O.S.; Taylor, L.W.; Trafford, M.A.; Yomogida, Y.; Wehmeyer, G.; Pasquali, M.; Yanagi, K.; Kono, J. Macroscopic weavable fibers of carbon nanotubes with giant thermoelectric power factor. *Nat. Commun.* **2021**, *12*, 4931. [[CrossRef](#)]
37. Nonoguchi, Y.; Nakano, M.; Murayama, T.; Hagino, H.; Hama, S.; Miyazaki, K.; Matsubara, R.; Nakamura, M.; Kawai, T. Simple salt-coordinated n-type nanocarbon materials stable in air. *Adv. Funct. Mater.* **2016**, *18*, 3021. [[CrossRef](#)]
38. Horike, S.; Wei, Q.; Akaike, K.; Kirihara, K.; Mukaida, M.; Koshihara, Y.; Ishida, K. Bicyclic-ring base doping induces n-type conduction in carbon nanotubes with outstanding thermal stability in air. *Nat. Commun.* **2022**, *13*, 3517. [[CrossRef](#)]
39. Seki, Y.; Nagata, K.; Takashiri, M. Facile preparation of air-stable n-type thermoelectric single-wall carbon nanotube films with anionic surfactants. *Sci. Rep.* **2020**, *10*, 8104. [[CrossRef](#)]
40. Nakashima, Y.; Yamaguchi, R.; Toshimitsu, F.; Matsumoto, M.; Borah, A.; Staykov, A.; Islam, M.S.; Hayami, S.; Fujigaya, T. Air-stable n-type single-walled carbon nanotubes doped with benzimidazole derivatives for thermoelectric conversion and their air-stable mechanism. *ACS Appl. Nano Mater.* **2019**, *2*, 4703. [[CrossRef](#)]
41. Amma, Y.; Miura, K.; Nagata, S.; Nishi, T.; Miyake, S.; Miyazaki, K.; Takashiri, M. Ultra-long air-stability of n-type carbon nanotube films with low thermal conductivity and all-carbon thermoelectric generators. *Sci. Rep.* **2022**, *12*, 21603. [[CrossRef](#)]
42. Hwang, H.; Jang, K.-S. Thermoelectric all-carbon heterostructures for a flexible thermoelectric generator. *Sustain. Energy Fuels* **2021**, *5*, 267–273. [[CrossRef](#)]
43. Lee, T.; Park, K.T.; Ku, B.-C.; Kim, H. Carbon nanotube fibers with enhanced longitudinal carrier mobility for high-performance all-carbon thermoelectric generators. *Nanoscale* **2019**, *11*, 16919–16927. [[CrossRef](#)]
44. Behabtu, N.; Young, C.C.; Tsentelovich, D.E.; Kleinerman, O.; Wang, X.; Ma, A.W.; Bengio, E.A.; Ter Waarbeek, R.F.; De Jong, J.J.; Hoogerwerf, R.E.; et al. Strong, light, multifunctional fibers of carbon nanotubes with ultrahigh conductivity. *Science* **2013**, *339*, 182. [[CrossRef](#)]
45. Seki, Y.; Takashiri, M. Freestanding bilayers of drop-cast single-walled carbon nanotubes and electropolymerized poly(3,4-ethylenedioxythiophene) for thermoelectric energy harvesting. *Org. Electron.* **2020**, *76*, 105478. [[CrossRef](#)]
46. Grosso, D. How to exploit the full potential of the dip-coating process to better control film formation. *J. Mater. Chem.* **2011**, *21*, 17033. [[CrossRef](#)]

47. Seki, Y.; Takahashi, M.; Takashiri, M. Effects of different electrolytes and film thicknesses on structural and thermoelectric properties of electropolymerized poly(3,4-ethylenedioxythiophene) films. *RSC Adv.* **2019**, *9*, 15957. [[CrossRef](#)]
48. Li, X.; Cai, K.; Gao, M.; Du, Y.; Shen, S. Recent advances in flexible thermoelectric films and devices. *Nano Energy* **2020**, *89*, 106309.
49. Zeng, F.; Zhao, X.; Luo, M.; Wang, W.; Qing, X.; Lu, Y.; Zhong, W.; Liu, Q.; Luo, L.; Li, M.; et al. A transparent PEDOT:PPS/PVA-co-PE/epoxy thermoelectric composite device with excellent flexibility and environmental stability. *Compos. Sci. Technol.* **2022**, *218*, 109153. [[CrossRef](#)]
50. Yu, P.; Feng, L.; Tang, W.; Liu, C.; Lan, J.-L.; Lin, Y.-H.; Yang, X. Robust, flexible thermoelectric film for energy harvesting by a simple and eco-friendly method. *ACS Appl. Mater. Interfaces* **2023**, *15*, 13144–13154. [[CrossRef](#)]
51. Kim, J.Y.; Ahn, K.; Jeong, S.Y.; Jeong, E.D.; Jin, J.S.; Bae, J.S.; Kim, H.G.; Cho, C.R. Enhancement of adhesion between polyphenylene sulfide and copper by surface treatments. *Curr. Appl. Phys.* **2014**, *14*, 118. [[CrossRef](#)]
52. Inagaki, N.; Narushima, K.; Morita, M. Plasma surface modification of poly(phenylene sulfide) films for copper metallization. *J. Adhes. Sci. Technol.* **2006**, *20*, 917–938.
53. Anagreh, N.; Dorn, L.; Bilke-Krause, C. Low-pressure plasma pretreatment of polyphenylene sulfide (PPS) surfaces for adhesive bonding. *Int. J. Adhes. Adhes.* **2008**, *28*, 16–22. [[CrossRef](#)]
54. Xu, D.; Yang, W.; Li, X.; Hu, Z.; Li, M.; Wang, L. Surface nanostructure and wettability inducing high bonding strength of polyphenylene sulfide-aluminum composite structure. *Appl. Surf. Sci.* **2020**, *515*, 145996. [[CrossRef](#)]
55. Nguyen, T.P.; Lahmar, A.; Jonnard, P. Adhesion improvement of poly(phenylene-vinylene) substrates induced by argon-oxygen plasma treatment. *J. Adhes.* **1998**, *66*, 303–317.
56. Carlson, E.J.; Strunz, K.; Otis, B.P. A 20 mV input boost converter with efficient digital control for thermoelectric energy harvesting. *IEEE J. Solid-State Circuits* **2010**, *45*, 741. [[CrossRef](#)]

Disclaimer/Publisher's Note: The statements, opinions and data contained in all publications are solely those of the individual author(s) and contributor(s) and not of MDPI and/or the editor(s). MDPI and/or the editor(s) disclaim responsibility for any injury to people or property resulting from any ideas, methods, instructions or products referred to in the content.